



This is a repository copy of *Satellite observations of Arctic blowing dust events >82°N*.

White Rose Research Online URL for this paper:

<https://eprints.whiterose.ac.uk/216468/>

Version: Accepted Version

Article:

Baddock, M. orcid.org/0000-0003-1490-7511, Hall, A. orcid.org/0009-0004-8857-7222, Rideout, J. et al. (3 more authors) (2025) Satellite observations of Arctic blowing dust events >82°N. *Weather*, 80 (2). pp. 61-66. ISSN 0043-1656

<https://doi.org/10.1002/wea.7617>

© 2024 The Authors. Except as otherwise noted, this author-accepted version of a journal article published in *Weather* is made available via the University of Sheffield Research Publications and Copyright Policy under the terms of the Creative Commons Attribution 4.0 International License (CC-BY 4.0), which permits unrestricted use, distribution and reproduction in any medium, provided the original work is properly cited. To view a copy of this licence, visit <http://creativecommons.org/licenses/by/4.0/>

Reuse

This article is distributed under the terms of the Creative Commons Attribution (CC BY) licence. This licence allows you to distribute, remix, tweak, and build upon the work, even commercially, as long as you credit the authors for the original work. More information and the full terms of the licence here:

<https://creativecommons.org/licenses/>

Takedown

If you consider content in White Rose Research Online to be in breach of UK law, please notify us by emailing eprints@whiterose.ac.uk including the URL of the record and the reason for the withdrawal request.



eprints@whiterose.ac.uk
<https://eprints.whiterose.ac.uk/>

1 **Satellite observations of Arctic blowing dust events >82°N**

2 Matthew Baddock*¹, Alex Hall¹, Joseph Rideout¹, Rob Bryant², Joanna Bullard¹ and
3 Santiago Gassó^{3,4}

4 ¹Department of Geography and Environment, Loughborough University, UK

5 ²Department of Geography, University of Sheffield, UK

6 ³Earth System Science Interdisciplinary Center, University of Maryland, College
7 Park, MD, USA

8 ⁴NASA Goddard Space Flight Center, Greenbelt, MD, USA

9

10

11 *corresponding author

12 m.c.baddock@lboro.ac.uk

13

14

15

16

17

18

19

20

21

22

23

24

25

26 **Abstract**

27 This study reports satellite evidence for the most northerly blown dust activity yet
28 observed on Earth. A systematic inspection of high-resolution satellite imagery
29 identified active dust events and their sources >82°N in Peary Land, Greenland. In
30 the absence of any local weather measurements, for all observed dust activity a
31 focus period in April 2020 with multiple dust plumes, reanalysis climate data found
32 the majority of dust events to be associated with windspeeds exceeding a typical
33 threshold value for blowing sand and dust uplift. Wind direction variability points to
34 dust-raising by cold airflow down-valley winds, likely from nearby ice masses.

35 **Keywords**

36 arctic weather; dust storms; mineral aerosols; CARRA

37 **Introduction**

38 Blowing dust is a common meteorological phenomenon in particular regions of the
39 world. Dust events constitute formal weather-types that are recordable within
40 synoptic observations, and whilst primarily associated with desert low latitudes, dust
41 activity has long been recognised at high latitudes (Bullard et al., 2016; Meinander et
42 al., 2022). The frequent strong winds of these environments, sparse vegetation cover
43 in cold temperatures and a plentiful supply of fine-sized sediment provide the
44 necessary conditions for dust uplift by aeolian (wind-driven) processes. In high
45 latitudes, dust activity is closely connected to current or former ice extent,
46 established partly by where fine sediment accumulates and also how ice masses
47 influence weather, for example, by generating katabatic winds (Bullard, 2013; Bullard
48 et al., 2016). Dust activity has environmental and societal significance wherever it
49 occurs (Okin et al., 2011; Middleton et al., 2017), and in the high latitudes its impacts
50 include air quality in settlements (e.g. Reykjavik, Thorsteinsson et al., 2011), nutrient
51 inputs to ecosystems (Anderson et al., 2017; Crusius, 2021) and a role in ice
52 nucleation and cloud formation as an influence on radiative budgets (Sanchez-
53 Marroquin et al., 2020; Shi et al., 2022; Barr et al., 2023). To understand the controls
54 on blowing dust, a key requirement is knowledge of the source areas from which
55 dust outbreaks occur. Whilst research in the low latitudes has successfully produced
56 satellite-based inventories of dust source locations (e.g. Baddock et al., 2011;
57 Vickery et al., 2013), evidence concerning the locations of dust activity at higher

58 latitudes, including the Arctic, is much less developed. This deficiency is partly due to
59 impediments on dust source monitoring at these latitudes, as associated with cloud
60 cover, seasonal polar darkness and the high-angle limitations of satellite sensors
61 (Bullard et al., 2016).

62 For high latitudes, another challenge is the lack of at-source weather data and
63 general sparseness of observations throughout regions. Such data availability is
64 compounded by the spatially constrained and remote location of areas likely to act
65 as sources of dust (Huck et al., 2023; Meinander et al., 2022). In fact,
66 micrometeorological measurements made directly at-source in dusty environments
67 are rare even in low latitudes and are usually only achieved by dedicated campaigns
68 (e.g. Wiggs et al., 2022). In place of widespread observations, the advent of climate
69 reanalysis data has been of considerable value for reconstructing the winds that lead
70 to blown dust, through the analysis of these time- and space-gridded datasets at
71 dust source locations. The recent Copernicus Arctic Regional Reanalysis (CARRA)
72 effort is one such dataset specially developed for the Arctic (Yang et al., 2020). In
73 particular, the high spatial resolution of CARRA (2.5 km) provides an enhanced way
74 to look at meteorological variables in topographically complex areas (Køltzow et al.,
75 2022). This is especially appropriate for dust studies at high latitudes because the
76 preferential source areas where dust outbreaks occur are often associated with
77 valley topography, as demonstrated by recent studies (e.g. Crusius 2021; van Soest
78 et al., 2022; Huck et al., 2023). The extent to which CARRA can be used to elucidate
79 dust emissions alongside satellite imagery remains an area of interest and, away
80 from the few instrumented locations, the spatial variation of where dust events occur,
81 when and how often they blow, represent important questions. The extent to which
82 sources of dust are distributed latitudinally is one aspect of this uncertainty. Ranjbar
83 et al. (2021) recently reported a case study of a dust outbreak near Lake Hazen in
84 Nunavut, Canada (latitude 81.67°N). To date, this has been the furthest north
85 satellite-based observation of blowing dust. Based on a review of high-resolution
86 satellite imagery, the current study reports new observations of dust phenomena
87 occurring >82°N in Greenland, with insights into the wind conditions associated with
88 this most northerly of dust activity.

89 **Methods**

90 To investigate dust occurrence in far-north Greenland, European Space Agency
91 (ESA) Sentinel-2 true-colour satellite imagery was systematically examined between
92 2016-2022 over 23 glacio-fluvial valleys $>82^{\circ}\text{N}$ that represent individual potential
93 dust sources in the Peary Land region. The $>82^{\circ}\text{N}$ sector focused on here was part
94 of a larger survey of dust sources in Greenland, based on Sentinel-2 due to the
95 ground detail its 10-m resolution visible bands provide. The selection of the 23
96 candidate sources for inspection in the region was based on a imagery-based survey
97 of valley topography containing identifiable loose sediment, as informed by the
98 characteristics of typical source areas that have been recognised elsewhere at high
99 latitudes (summarised by Bullard et al. (2016)). Imagery from Sentinel-2 is only
100 routinely available to about 82.5°N and the coverage of potential sources inspected
101 in the latitudinal band $82\text{-}82.5^{\circ}\text{N}$ is shown in Figure 1. Using facilities available in the
102 freely available Copernicus Data Space Ecosystem
103 (<https://browser.dataspace.copernicus.eu/>), criteria were set to sample one image
104 per day from Sentinel-2A/B, and to include all scenes with $<65\%$ cloud but $>50\%$
105 coverage of Sentinel image tile. The resulting imagery catalogue generated over
106 each candidate source (typically >600 images over the 7-year period) was then
107 manually inspected for the appearance of dust plumes.

108 For the 23 candidate dust sources systematically examined above 82°N , dust was
109 observed at two locations in the Wandel Dal valley, at 82.22°N (Source A) and
110 82.19°N (Source B) (Figure 1). For Source A there were 13 different dates of dust
111 detection over the seven-year study, and at Source B only a single date showed
112 dust. CARRA reanalysis data were then obtained for all dust-observed dates, as well
113 as a multi-day period to examine the most active dust period at Source A. CARRA
114 variables are available 3-hourly and were obtained for windspeed, wind direction
115 (both 10-m height) and 2-m air temperature. The modelled CARRA windspeed
116 product has previously been tested in the north-eastern European Arctic and
117 performed well against observations demonstrating an improvement for the region
118 over ERA5, for example in capturing winds of polar lows (Køltzow et al., 2022).
119 Accurately representing wind fields in complex topography can be a challenge for
120 reanalysis products and Køltzow et al. (2022) report that the largest departure of
121 CARRA from observed windspeeds is seen for sites such as coastal fjords which
122 have some similarity to the terrestrial Wandel Dal valley landscape.

123 <<Figure 1>>

124 A key meteorological control on dust activity is exceedance of a threshold windspeed
125 required for dust uplift. Estimates of threshold values are scarce for high latitude
126 environments, but saltation (the hopping behaviour of sand grains along the surface
127 during their wind-blown transport) is a recognised driving process of dust emission,
128 related to sandblasting of the surface which liberates dust (Shao et al., 1993). If dry
129 sediment of a typical sand grain size is assumed, a 10-m windspeed of $\sim 6 \text{ m s}^{-1}$ is a
130 realistic lower value for saltation and thereby dust uplift (Bagnold, 1941). Such a
131 windspeed magnitude was specifically linked to dust suspension in the
132 Kangerlussuaq valley, south-west Greenland (Dijkmans and Törnqvist, 1991).

133 **Results**

134 For the two sources observed in Wandel Dal, the dates of observed dust represent a
135 rate of 1.9 events per year for Source A (82.22°N), and 0.14 per year for Source B
136 (82.19°N) (Figure 1). At Source A, the systematic examination of imagery showed
137 blowing dust on three different springtime days in the last third of April 2020 (19th,
138 20th and 25th), exemplified in Figure 2bcd. One benefit for monitoring sites at
139 extremely high latitudes is the multiple overpasses occurring each day for any given
140 location due to overlapping coverage of low-Earth orbit satellites like Sentinel-2A/B
141 (overpass record in Figure 3a) (Baddock et al., 2021). On 19th April, dust was seen
142 blowing in all three overpasses that day, over the period 1759-1939 (all times UTC).
143 Likewise, for the four overpasses on 20th April, all imagery showed observable dust,
144 and again from 1728-1819 on 25th April. For a focused period of 17-25th April, a look
145 at all available Sentinel-2 imagery (i.e. all overpasses each day and including those
146 scenes with >65% cloud, originally excluded in the initial review) identified a further
147 date with dust apparent (24th April, at 1849 and 1938). The high frequency of satellite
148 overpass through this April period provided a clear record of occasional but repeated
149 blowing dust. This cluster of events was also examined for the relationship between
150 CARRA wind variability and satellite-observed dust for April 17-25th.

151 <<Figure 2>>

152 Linking the reanalysis data to the times when blowing dust was seen (and
153 conversely, satellite overpasses *without* dust), the CARRA windspeed record helps
154 account for three of the observed dust outbreaks (Figure 3a). The dust observations

155 on 19th and 20th April both coincided with mean windspeeds (spatially averaged over
156 the source) that well exceeded the indicative threshold of 6 m s⁻¹, reaching 7.9 (with
157 a 8.5 m s⁻¹ local maximum) and 9.1 m s⁻¹ (9.2 m s⁻¹ local maximum) respectively at
158 1800, nearest to overpass times. For the other two dates of observed dust, while the
159 source-averaged windspeeds at 1800 were sub-threshold on the 24th and 25th, at 5.2
160 and 4.7 m s⁻¹, the local maximum speed over the source at 1800 on each day was
161 6.5 and 5.3 m s⁻¹. These maxima indicate that at the 2.5 km resolution of the CARRA
162 grid, winds were above threshold over at least part of the Source A area on the 24th,
163 and the plume observed at lower windspeeds on 25th is indeed smaller than the
164 previous days' dust outbreaks (Figure 2d).

165 <<Figure 3>>

166 The wider relationship between blowing dust and the 6 m s⁻¹ threshold can also be
167 summarised across all dates when dust was observed from Sources A and B, as
168 examined for 2016-22. For the 14 observed dust dates, the multiple Sentinel-2
169 overpasses that occur per day as exemplified in Figure 3, meant that based on the
170 overpass timing, CARRA windspeeds from 23 individual 3-hourly times (either from
171 1800 or 2100 UTC) could be examined. For these 23 instances, the mean
172 windspeed spatially averaged over the source nearest in time to a Sentinel-2 dust
173 observation was 6.6 m s⁻¹, while the mean maximum windspeed over source was 7.3
174 m s⁻¹. In terms of spatially averaged windspeeds, 65% of the dust-linked times were
175 greater than 6 m s⁻¹, while the local maximum windspeed was seen to exceed the
176 assumed threshold for 70% of dust events.

177 Wind direction from CARRA matches the observed dust plume directions well for all
178 outbreaks. Figure 3 indicates that three of the four observed dust events were down-
179 valley (broadly westerly) winds, with dust plumes extending over the bordering lake
180 body (Midsommersø) east of the source. The most developed plume was that seen
181 at 1819 20th April where dust had extended >5 km over the lake (Figure 2c),
182 corresponding well with reanalysis wind direction of 250° at 1800. On 25th April winds
183 from ~105° agreed with plumes imaged as heading up-valley (Figure 2d).

184 **Discussion**

185 Different methodologies of determining dust event frequency make comparisons
186 between places (and studies) difficult, but 1.9 events per year at Source A is

187 comparable with frequencies of dust-coded daily weather observations found at
188 some low-latitude desert margins (Engelstaedter et al., 2003). Despite such
189 frequency being considered “per year”, the window for likely dust activity from these
190 high latitude sources is not a fully annual period, and there is reduced (or even zero)
191 potential for dust activity through much of the year. Other studies have for instance
192 shown that most high-latitude sources preferentially experience dust in the spring
193 (e.g. later April, Figure 3), after winter snow cover has melted, but before valleys
194 undergo inundation by summer meltwater flooding (Bullard et al., 2016). This pattern
195 has been shown in southwest Greenland from dust-associated weather codes
196 reported at Kangerlussuaq airport (67°N) (Bullard and Mockford, 2018). Snow-free
197 valley surfaces before extensive meltwater inundation are evident in Figure 2,
198 indicating the susceptibility of these springtime surfaces to yield dust when winds
199 exceed threshold. Autumn periods, after summer melt has ceased and before the
200 arrival of snow, also establish similar conditions (e.g. in Copper River of Alaska
201 (Crusius et al., 2011)) and two of the 13 Source A events were observed in
202 September. Furthermore, because the number of days when any given source can
203 be effectively monitored for dust by satellites such as Sentinel-2 is variable – as
204 controlled by satellite orbit paths, times of overpass/dust, polar night (~6 months of
205 the year at 82°N, from mid-September to late March), and the variable presence of
206 cloud obscuring the surface - the Sentinel-based annual frequency represents an
207 unknown but undoubted underestimation of dust frequency at these >82°N sources.
208 Regardless of the uncertainty surrounding the true frequency of blowing dust and the
209 ability of satellites to accurately determine this (Bullard et al., 2016), our satellite
210 analysis provides clear evidence of newly recognised dust activity at such latitudes.

211 This study also demonstrates how satellite observations establish known times of
212 raised dust that can help determine wind’s role in causing dust events. For example,
213 the occurrence of three of the four captured events being associated with reanalysis
214 winds >6 m s⁻¹ in Figure 3a, and mean or maximum winds exceeding threshold for
215 65% or 70% of all dust observation times respectively, provides some confidence for
216 predicting dust over the period considered here. As winds will be spatially variable
217 inside topographic valleys it is not surprising that use of the maximum wind finds
218 better agreement with the evidence of active dust blowing.

219 The onset of the first period of dust activity over the 19-20th April saw mean
220 windspeed increase from 2.0 m s⁻¹ at 2100 on 18th April to 11.1 m s⁻¹ six hours later,
221 associated with an abrupt switch from easterly to down-valley north-westerly flow
222 (Figure 3a). This rapid wind acceleration with direction change occurred with a
223 temperature drop of 6°C over the same period (Figure 3b), indicating the fast airflow
224 was likely associated with cold air draining down the valleys leading from the ice
225 mass <20 km to the northwest of Wandel Dal (Figure 1), as also seen for the
226 Canadian Lake Hazen case (Ranjbar et al., 2021). A similar abrupt direction shift
227 also occurred with the windspeed increase that produced the down-valley dust
228 observed on 24th April, again linking this dust outbreak to katabatic winds.

229 The case of up-valley dust occurring at sub-threshold windspeeds on 25th April poses
230 an interesting question (Figure 3a). Bullard et al. (2023) reported episodes of
231 elevated dust concentration associated with up-valley wind directions at relatively
232 low windspeeds from measurements in the Kangerlussuaq valley, possibly from
233 further upwind sources in the same valley, but this is not the case here. The images
234 show active dust emission from Source A, and while dust observed under weaker
235 winds may be indicative of surfaces becoming more susceptible to erosion (where
236 dust can be lifted at lower windspeeds e.g. due to surface drying) a likely explanation
237 is that a single threshold does not characterise adequately the erodibility of the entire
238 source surface (McKenna Neuman, 1993). There is a suggestion that the CARRA
239 reanalysis has under-predicted the windspeeds at the time of dust observation (1800
240 UTC) on the 25th, or that the work of wind gusts in raising sediment is not reflected in
241 the 3-hourly timestep. Mean windspeeds of similar sub-threshold magnitude (~4-5 m
242 s⁻¹) on preceding days of the 18th and 23rd April did not produce dust, and since the
243 surface on those recent days can be expected to have been of similar erodible
244 potential to its state on the 25th, CARRA may not be representing true wind
245 strength... It is clear overall however that synergistic satellite observations and
246 CARRA reanalysis unambiguously document the role of winds directed both up- and
247 down-valley in raising dust; a characteristic behaviour also seen in other high latitude
248 valley dust sources over longer term field-based studies (e.g. Bullard et al., 2023).
249 The observation of such bi-directional dust activity is significant because the
250 transport direction of the raised dust will influence its impact following eventual

251 downwind deposition; for example as an aquatic nutrient input (Crusius, 2021) or via
252 its effect in albedo-darkening of snow and ice (Oerlemans et al., 2009).

253 **Conclusion**

254 While it is recognised that high latitude locations can be receptors of long-range dust
255 that originated in the low-latitudes (e.g. VanCuren et al, 2012), significance has
256 recently been attached to dust sources active in the high latitudes due to the links
257 between these sources and the fundamental properties of the suspended dust which
258 govern its environmental impacts. For example, both the particle size distribution and
259 geochemistry of dust differ between high latitude locally-sourced dust and that which
260 has undergone a longer residence time in atmospheric transport (e.g, Shi et al.,
261 2020; Barr et al., 2023). For the sources examined here >82°N in Greenland, whilst
262 relatively small in spatial extent, the dust events reported in this study provide clear
263 evidence of the most northerly occurrences of blowing dust phenomena yet
264 observed on Earth. With the absence of meteorological observations from such
265 locations, when high-resolution satellite imagery is coupled with gridded regional
266 reanalysis data, such a combination of weather monitoring can offer insights into the
267 meteorological controls of dust processes that are active in these most extreme and
268 remote latitudes.

269 **Acknowledgements**

270 The authors are grateful for this research's funding from the European Space
271 Agency-Future Earth Joint Program (ESA-2022-02) and the organisational help of
272 Sophie Hebden. Through Future Earth, this work was undertaken under the auspices
273 of the Surface Ocean – Lower Atmosphere Study (SOLAS) project, where SOLAS is
274 itself partially supported by the U.S. National Science Foundation (Grant OCE-
275 1840868) via the Scientific Committee on Oceanic Research (SCOR). We thank the
276 EU Copernicus, Data Space Ecosystem for distribution of Sentinel-2 data and its
277 Climate Change Service for CARRA data. We thank the two anonymous reviewers
278 for helpful improvements and the Co-Editor-in-Chief, Simon Lee.

279 **Data Availability**

280 Sentinel-2 and CARRA data are freely available from EU Copernicus sources. The
281 point sources of surveyed candidate dust sources are available by request to the
282 corresponding author.

283 **Author Contributions**

284 Matthew Baddock: Conceptualisation, Writing – Original Draft, Visualisation, Formal
285 analysis, Funding acquisition, Validation, Supervision. Alex Hall: Investigation,
286 Formal Analysis, Data curation, Validation; Joe Rideout: Investigation, Formal
287 Analysis, Data curation, Validation; Rob Bryant: Conceptualisation, Writing – Review
288 and Editing, Visualisation, Formal analysis, Funding acquisition, Supervision,
289 Validation. Jo Bullard: Conceptualisation, Funding acquisition, Supervision,
290 Validation. Santiago Gassó: Conceptualisation, Writing – Review and Editing,
291 Funding acquisition, Supervision.

292 **References**

- 293 Anderson, N.J., & 26 others (2017) The Arctic in the 21st century: changing
294 biogeochemical linkages across a paraglacial landscape of Greenland. *BioScience*,
295 67(2), 118-133. <https://doi.org/10.1093/biosci/biw158>
296
- 297 Baddock, M. C., Gill, T.E, Bullard, J.E. Dominguez Acosta, M., and Rivera Rivera N.I.
298 (2011), A geomorphic map of the Chihuahuan Desert, North America, based on
299 potential dust emissions, *Journal of Maps*, 2011, 249–259,
300 doi:10.4113/jom.2011.1178
301
- 302 Baddock, M.C., Bryant, R.G., Dominguez Acosta, M. and Gill, T.E. (2021)
303 Understanding dust sources through remote sensing: Making a case for CubeSats.
304 *Journal of Arid Environments*, 184: 104335. doi:10.1016/j.jaridenv.2020.104335
305
- 306 Bagnold, R.A. (1941) *The Physics of Blown Sand and Desert Dunes*. London:
307 Methuen.
308
- 309 Barr, S.L., Wyld, B., McQuaid, J.B., Neely III, R.R. and Murray, B.J. (2023) Southern
310 Alaska as a source of atmospheric mineral dust and ice-nucleating particles. *Science*
311 *Advances*, 9, eadg3708. doi:10.1126/sciadv.adg3708
312
- 313 Bullard, J.E. (2013) Contemporary glacial inputs to the dust cycle. *Earth Surface*
314 *Processes and Landforms*, 38, 71-89. doi:10.1002/esp.3315
315

- 316 Bullard, J.E. & Mockford, T. (2018) Seasonal and decadal variability of dust
317 observations in the Kangerlussuaq area, West Greenland. *Arctic, Antarctic, and*
318 *Alpine Research*, 50, S100011. doi:10.1080/15230430.2017.1415854
319
- 320 Bullard, J.E., & 13 others (2016) High-Latitude dust in the Earth system. *Reviews of*
321 *Geophysics*, 54, 447-485. doi:10.1002/2016RG000518
322
- 323 Bullard, J.E., Prater, C., Baddock, M.C., and Anderson, N.J. (2023) Diurnal and
324 seasonal source-proximal dust concentrations in complex terrain, West Greenland.
325 *Earth Surface Processes and Landforms*, 48, 2808-2827. doi:10.1002/esp.5661
326
- 327 Crusius, J. (2021) Dissolved Fe supply to the central Gulf of Alaska is inferred to be
328 derived from Alaskan glacial dust that is not resolved by dust transport models. *Journal*
329 *of Geophysical Research - Biogeosciences*, 126, e2021JG006323,
330 doi:10.1029/2021JG006323
331
- 332 Crusius, J., Schroth, A.W., Gassó, S., Moy, C.M., Levy, R.C. and Gatica, M. (2011),
333 Glacial flour dust storms in the Gulf of Alaska: Hydrologic and meteorological
334 controls and their importance as a source of bioavailable iron. *Geophysical Research*
335 *Letters*, 38, L06602. doi:10.1029/2010gl046573
336
- 337 Dijkmans, J.W.A. & Törnqvist, T.E. (1991) Modern periglacial eolian deposits and
338 landforms in the Søndre Strømfjord area, West Greenland and their
339 palaeoenvironmental implications. *Meddelelser om Grønland, Geoscience*, 25, 3-39.
340
- 341 Engelstaedter, S., K. E. Kohfeld, I. Tegen, and S. P. Harrison (2003), Controls of dust
342 emissions by vegetation and topographic depressions: An evaluation using dust
343 storm frequency data, *Geophysical Research Letters*, 30, 1294,
344 doi:10.1029/2002GL016471
345
- 346 Huck, R., Bryant, R.G. and King, J. (2023) The (mis)identification of high-latitude
347 dust events using remote sensing methods in the Yukon, Canada: a sub-daily
348 variability analysis. *Atmospheric Chemistry and Physics*, 23, 6299-6318.
349 doi:10.5194/acp-23-6299-2023
350
- 351 Køltzow, M., Schyberg, H., Støylen, E., and Yang, X. (2022) Value of the Copernicus
352 Arctic Regional Reanalysis (CARRA) in representing near-surface temperature and
353 wind speed in the north-east European Arctic. *Polar Research*, 41. doi:
354 10.33265/polar.v41.8002
355
- 356 McKenna Neuman, C. (1993) A review of aeolian transport processes in cold
357 environments. *Progress in Physical Geography*, 17, 137-155.
358

- 359 Meinander, O. and 55 others (2022) Newly identified climatically and environmentally
360 significant high-latitude dust sources, *Atmospheric Chemistry and Physics*, 22,
361 11889–11930, doi:10.5194/acp-22-11889-2022
362
- 363 Middleton, N.J. (2017) Desert dust hazards: a global review. *Aeolian Research*, 24,
364 53-63. doi: 10.1016/j.aeolia.2016.12.001
365
- 366 Oerlemans, J., Giesen, R.H., van den Broeke, M.R., 2009. Retreating alpine
367 glaciers: increased melt rates due to accumulation of dust (Vadret da Morteratsch,
368 Switzerland). *Journal of Glaciology*, 55, 729–736. doi:10.3189/00221430978947096
369
- 370 Okin G.S. & 9 others (2011) Dust emission: small-scale processes with global-scale
371 consequences. *Eos, Transactions of the American Geophysical Union*, 92: 241–242.
372 doi:10.1029/2011EO290001
373
- 374 Ranjbar, K., O'Neill, N.T., Ivanescu, L., King, J. and Hayes, P.L. (2021) Remote
375 sensing of a high-Arctic, local dust event over Lake Hazen (Ellesmere Island,
376 Nunavut, Canada). *Atmospheric Environment*, 246, 118102.
377 doi:10.1016/j.atmosenv.2020.118102
378
- 379 Sanchez-Marroquin, A., Arnalds, O., Baustian-Dorsi, K. J., Browse, J., Dagsson-
380 Waldhauserova, P., Harrison, A. D., Maters, E.C., Pringle, K. J., Vergara-Temprado,
381 J., Burke, I. T., McQuaid, J. B., Carslaw, K. S., and Murray, B. J. (2020) Iceland is an
382 episodic source of atmospheric ice-nucleating particles relevant for mixed-phase
383 clouds, *Science Advances*, 6, eaba8137, doi:10.1126/sciadv.aba8137, 2020
384
- 385 Shao, Y., Raupach, M.R. and Findlater, P.A. (1993) Effect of saltation bombardment
386 on the entrainment of dust by wind. *Journal of Geophysical Research*, 98, D&,
387 12719-12726
388
- 389 Shi, Y., Liu, X., Wu, M., Zhao, X., Ke, Z., and Brown, H. (2022) Relative importance
390 of high-latitude local and long-range-transported dust for Arctic ice-nucleating
391 particles and impacts on Arctic mixed-phase clouds, *Atmospheric Chemistry and
392 Physics*, 22, 2909–2935. doi:10.5194/acp-22-2909-2022
393
- 394 Thorsteinsson, Th., Gísladóttir, G., Bullard, J. & McTainsh, G. (2011). Dust storm
395 contributions to airborne particular matter in Reykjavík, Iceland. *Atmospheric
396 Environment*, 45, 5924-5933. doi:10.1016/j.atmosenv.2011.05.023
397
- 398 van Soest, M.A.J., Bullard, J.E., Prater, M.C., Baddock, M.C. & Anderson, N.J.
399 (2022), Annual and seasonal variability in high latitude dust deposition, West
400 Greenland. *Earth Surface Processes and Landforms*. doi:10.1002/esp.5384
401

- 402 VanCuren, R. A., T. Cahill, J. Burkhart, D. Barnes, Y. Zhao, K. Perry, S. Cliff, and J.
403 McConnell (2012), Aerosols and their sources at Summit
404 Greenland—First results of continuous size- and time-resolved sampling,
405 Atmospheric Environment, 52, 82–97. doi:10.1016/j.atmosenv.2011.10.047.
406
- 407 Vickery, K.J., Eckardt, and R.G. Bryant (2013) A sub-basin scale dust plume source
408 frequency inventory for southern Africa, 2005-2008, *Geophysical Research Letters*,
409 40, 5274-5279, doi:10.1002/grl.50968
410
- 411 Wiggs, G.F.S. & 9 others (2022) Quantifying mechanisms of aeolian dust emission:
412 field measurements at Etosha Pan, Namibia. *Journal of Geophysical Research –*
413 *Earth Surface*, 127, e2022JF006675. doi:10.1029/2022JF006675
414
- 415 Yang, X., & 19 others (2020) C3S Arctic Regional Reanalysis – Full system
416 documentation. [https://datastore.copernicus-climate.eu/documents/reanalysis-](https://datastore.copernicus-climate.eu/documents/reanalysis-carra/CARRAFullSystemDocumentationFinal.pdf)
417 [carra/CARRAFullSystemDocumentationFinal.pdf](https://datastore.copernicus-climate.eu/documents/reanalysis-carra/CARRAFullSystemDocumentationFinal.pdf)

418

419

420

421

422

423

424

425

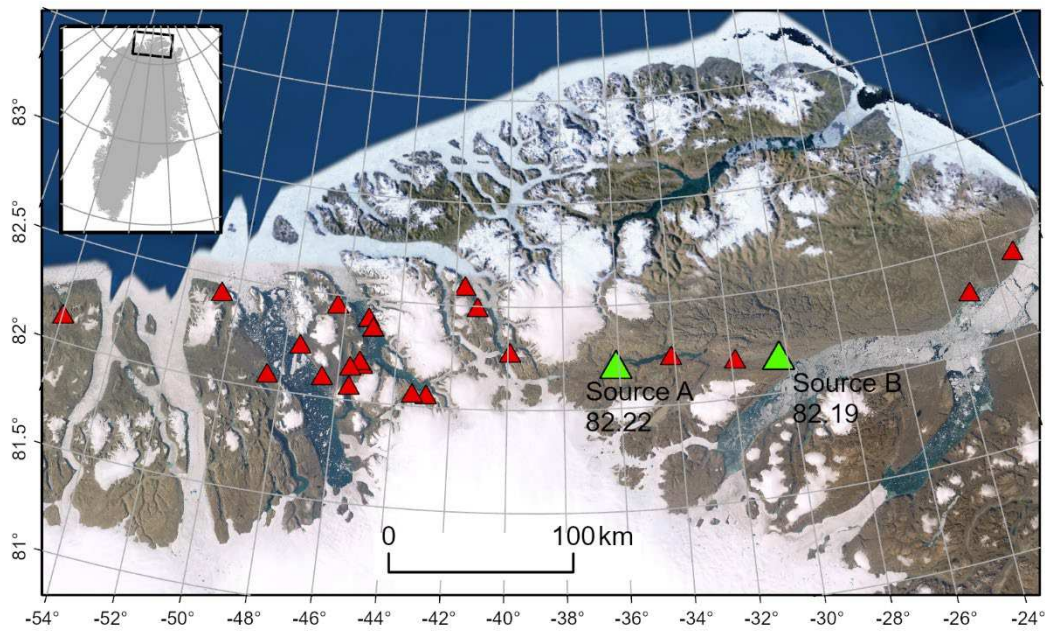
426

427

428

429

430 **Figures**



431

432 Figure 1: The study area of Peary Land, northern Greenland, showing all candidate
433 dust source locations inspected >82°N. Candidate locations not exhibiting any
434 observable dust activity in the 2016-2022 systematic review of Sentinel-2 imagery
435 are marked red, while the two locations where dust events were observed are green
436 and labelled (Source A and B). Underlying image is the ESRI-provided World
437 Imagery high resolution basemap for 2021-09-1.

438

439

440

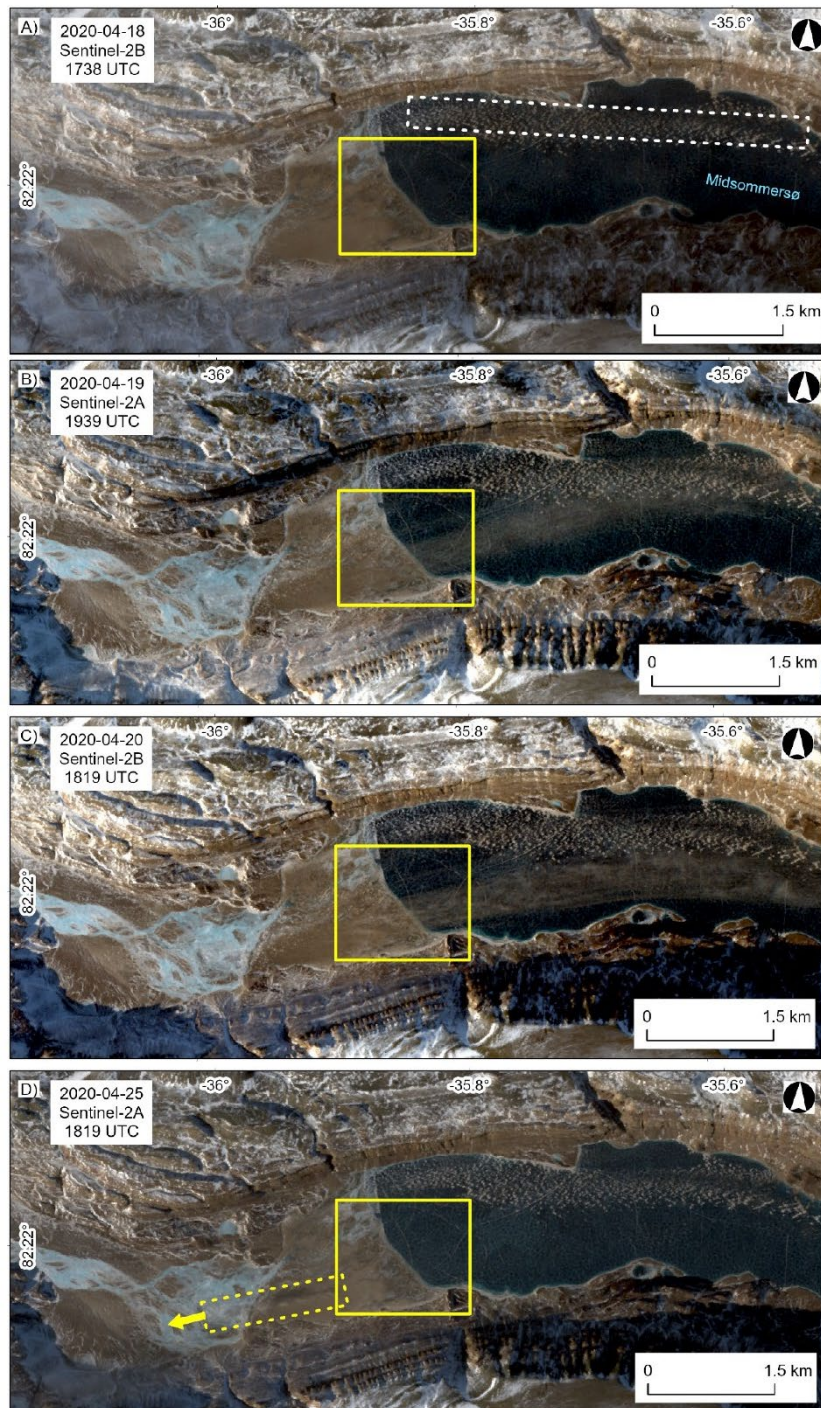
441

442

443

444

445

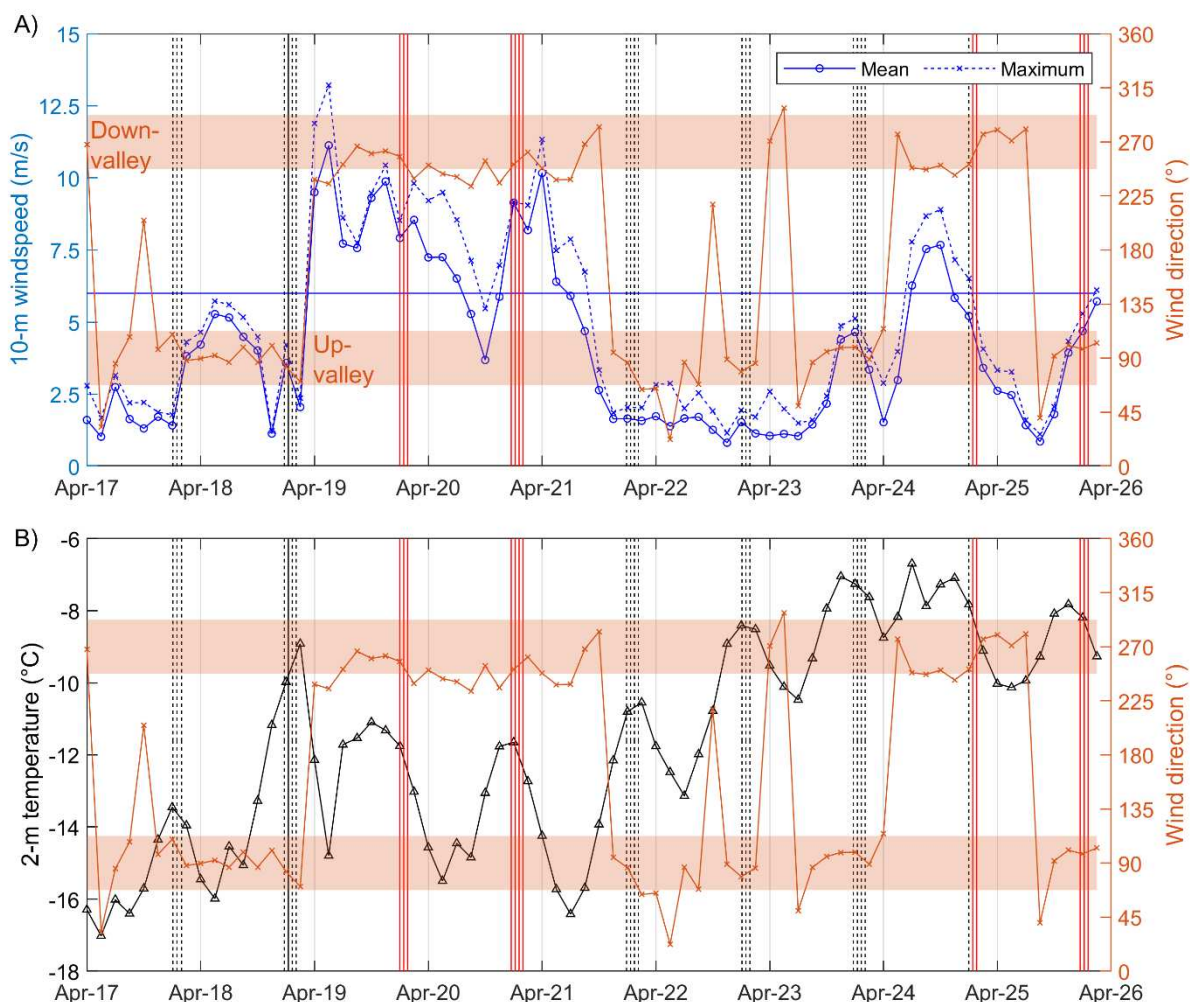


446

447 Figure 2: Sentinel-2 true-colour images over Source A for selected days from the
448 focused study period in late April 2020. A) Dust-free scene on April 18th, B) down-
449 valley dust event captured on April 19th, C) well developed dust plume extending
450 over the source-bordering lake (Midsommørsø), to the east, April 20th, D) small up-
451 valley directed dust plume (marked by dashed yellow box and arrow) on April 25th
452 The dashed white box in A highlights presence of drifted snow formed on the surface
453 of the frozen lake, with brown appearance likely due to recent previous dust

454 deposition. The common yellow box highlights the land surface area containing the
455 upwind points of observed dust plumes for comparison with the dust-free scene.

456



457

458 Figure 3: A) Time series of spatially-averaged mean windspeed, single-point
459 maximum windspeed and wind direction all at 10 m, and B) 2-m air temperature
460 together with 10-m wind direction, from 3-hourly CARRA reanalysis, for Source A
461 through the period 17-25th April 2020. The straight horizontal line in the top panel
462 shows a 6 m s⁻¹ indicative threshold for aeolian activity. Vertical lines in both panels
463 indicate all overpass times of Sentinel-2A/B, where black dash indicates overpass
464 with no dust plume visible (19), red indicates dust plume visible (12) and black solid
465 indicates a cloud-obscured scene (1). The upper horizontal peach patch highlights

466 down-valley wind directions from WNW-WSW, and lower patch marks up-valley
467 winds from ENE-ESE.